

Half-metallicity and Gilbert damping constant in $\text{Co}_2\text{Fe}_x\text{Mn}_{1-x}\text{Si}$ Heusler alloys depending on the film composition

著者	安藤 康夫
journal or publication title	Applied Physics Letters
volume	94
number	12
page range	122504-1-122504-3
year	2009
URL	http://hdl.handle.net/10097/46377

doi: 10.1063/1.3105982

Half-metallicity and Gilbert damping constant in $\text{Co}_2\text{Fe}_x\text{Mn}_{1-x}\text{Si}$ Heusler alloys depending on the film composition

Takahide Kubota,^{1,a)} Sumito Tsunegi,¹ Mikihiro Oogane,¹ Shigemi Mizukami,² Terunobu Miyazaki,² Hiroshi Naganuma,¹ and Yasuo Ando¹

¹Department of Applied Physics, Graduate School of Engineering, Tohoku University, Aza-aoba 6-6-05, Aramaki, Aoba-ku, Sendai 980-8579, Japan

²WPI Advanced Institute for Materials Research, Tohoku University, Katahira 2-1-1, Aoba-ku, Sendai 980-8577, Japan

(Received 29 January 2009; accepted 4 March 2009; published online 24 March 2009)

Transport properties in magnetic tunnel junctions (MTJs) with $\text{Co}_2\text{Fe}_x\text{Mn}_{1-x}\text{Si}$ (CFMS, $x=0-1.0$)/Al–O/ $\text{Co}_{75}\text{Fe}_{25}$ structure and Gilbert damping constant in the epitaxial CFMS films were investigated. The tunnel magnetoresistance ratio is as high as 75% in MTJs with $x=0.6$ at room temperature. The Gilbert damping constant is minimal at $x=0.4$. Relations between half-metallicity and the Gilbert damping constant in CFMS films were examined, revealing that the damping constant is small in *half-metallic* CFMS films. © 2009 American Institute of Physics.

[DOI: 10.1063/1.3105982]

Half-metallic ferromagnets (HMFs) are an ideal material for “spintronics” applications because they have an energy gap at the Fermi level only in the up or down spin channel, which enable to generate completely spin-polarized conduction electrons. Actually, Co-based full Heusler alloys are promising candidates as HMFs based on both *ab initio* calculations^{1,2} and some experimental results in magnetic tunnel junctions (MTJs) with such Heusler compounds’ electrodes.³⁻⁵ Among the Heuslers, Co_2MnSi and Co_2FeSi are suitable for device applications because of their high respective Curie temperatures: 985 K (Ref. 6) and 1100 K.⁷ Regarding half-metallicity, that characteristic of Co_2MnSi has been investigated experimentally in earlier reports.³⁻⁵ In the case of Co_2FeSi , both half-metallic⁸ and non-half-metallic¹ predictions have been described theoretically in earlier reports. Kandpal *et al.*⁸ reported a half-metallic band structure of Co_2FeSi by local spin density approximation and generalized gradient approximation treatment, including optimum effective Coulomb exchange interaction (U_{eff}). Galanakis *et al.*² reported the non-half-metallic nature of Co_2FeSi by the full-potential screened Korringa–Kohn–Rostoker Green’s function method. Experimentally, we have reported non-half-metallic TMR effect and transport properties in MTJs with a $\text{Co}_2\text{FeSi}/\text{Al}-\text{O}/\text{Co}_{75}\text{Fe}_{25}$ structure.⁹ On the other hand, studies on spin dynamics in *half-metallic* materials are also current topics.¹⁰⁻¹³ Among them, the Gilbert damping constant (α) in Co-based full Heusler alloys are attracted because quite small α in half-metallic Co_2MnSi has been reported.¹² Small α can be an advantage for the reduction in critical current density (J_c) in current-induced magnetization switching.¹²

As presented above, half-metallicity in Co_2FeSi is still under discussion; however, presuming that Co_2FeSi is not a half-metal, there is apparently a half-metallic transition point between Co_2MnSi and Co_2FeSi depending on their composition. Substitution of Mn to Fe would increase the Curie temperature of the Heusler alloy: at a certain Fe concentra-

tion of x , the $\text{Co}_2\text{Fe}_x\text{Mn}_{1-x}\text{Si}$ Heusler alloy can be a superior half-metallic material with higher Curie temperature than that of Co_2MnSi . As described in this letter, we investigated the half-metallicity in $\text{Co}_2\text{Fe}_x\text{Mn}_{1-x}\text{Si}$ (CFMS) Heusler alloys by observing transport properties in MTJs with the CFMS/Al–O/ $\text{Co}_{75}\text{Fe}_{25}$ structures and Gilbert damping constant of CFMS films.

All films were prepared using an inductively coupled plasma-assisted sputtering system equipped with ultrahigh vacuum chambers ($P_{\text{base}} < 2 \times 10^{-7}$ Pa). The stacking structure of MTJs is a single crystalline MgO (001) substrate/Cr (40 nm)/CFMS (30 nm)/Al (1.3 nm)–O/ $\text{Co}_{75}\text{Fe}_{25}$ (5 nm)/ $\text{Ir}_{22}\text{Mn}_{78}$ (10 nm)/Ta (5 nm), where the numbers in parentheses are film thicknesses in nanometers. After deposition of Cr and CFMS, postdeposition annealing was performed, respectively, at 700, and 500 °C (400 °C only for $x=0.8$ and 1.0). Compositions of CFMS films were controlled by cosputtering from $\text{Co}_{2.00}\text{Mn}_{1.28}\text{Si}_{1.30}$ and $\text{Co}_{2.00}\text{Fe}_{1.02}\text{Si}_{1.19}$ alloyed targets. We prepared samples with Fe concentration x of 0–1.0 at intervals of 0.2. Films were patterned into pillars of $10 \times 10-100 \times 100 \mu\text{m}^2$ using photolithography and Ar ion milling techniques. The TMR ratio of the MTJs was measured using a dc four-probe technique, with differential conductance dependence on applied bias voltage evaluated using a nanovoltmeter (model 2182A; Keithley Instruments, Inc.) and a small current source (model 6221; Keithley Instruments, Inc.). Furthermore, half-MTJ structures of MgO (001) substrate/Cr/CFMS/Ta (2 nm) were prepared for evaluations of crystalline structure, magnetic properties, and the Gilbert damping constant, which were evaluated, respectively, using x-ray diffractometry (XRD), a superconducting quantum interference device, and ferromagnetic resonance (FMR).

The results shown for XRD measurements confirmed the $B2$ and $L2_1$ site ordering for all Fe concentrations x in $\text{Co}_2\text{Fe}_x\text{Mn}_{1-x}\text{Si}$. Here we will not discuss the magnitude of $L2_1$ and $B2$ long range order parameters (S_{L2_1} and S_{B2}) because the difference in atomic number is only 1 between Co and Fe. Therefore detection and quantitative discussion of Co–Fe swapping ratio are quite difficult by XRD measurements. If we estimate them, $S_{B2}=0.9$ and $S_{L2_1}=0.8$ for

^{a)}Author to whom correspondence should be addressed. Electronic mail: takahide@mlab.apph.tohoku.ac.jp.

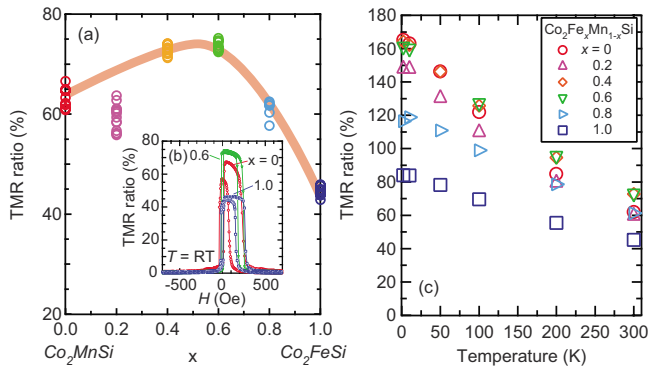


FIG. 1. (Color online) (a) TMR ratio in CFMS/Al–O/Co₇₅Fe₂₅ MTJs depending on the Fe concentration x in CFMS; inset (b) depicts typical TMR- H curve for the MTJs with $x=0$, 0.6, and 1.0; (c) shows the temperature dependence of TMR ratio in the MTJs with the CFMS electrode.

Co₂MnSi, and $S_{B2}=0.5-0.8$ and $S_{L2_1}=0.2-0.9$ for other CFMS films. Saturation magnetizations of Co₂MnSi ($x=0$) and Co₂FeSi ($x=1.0$) were, respectively, 800 and 1015 emu/cm³. These values were 20% lower than reported values for bulk samples,⁷ although magnetization increased systematically with increasing x . Detailed structural and magnetic properties were described in an earlier report.¹³

The dependence of the TMR ratio on the film composition of the CFMS is presented in Fig. 1(a). The inset depicts a typical TMR- H curve for MTJs with $x=0$, 0.6, and 1.0 at room temperature [Fig. 1(b)]. The TMR ratio exhibits a maximum around $x=0.4$ and 0.6. The highest value of the TMR ratio is 75% for the MTJs with Co₂Fe_{0.6}Mn_{0.4}Si electrode. It is a sufficiently higher value than that in Co₂MnSi (67%) and Co₂FeSi (46%). Correlations were not found between long range order parameters (S_{L2_1} and S_{B2}) and TMR ratio within the current sample series. That is, because of that, to achieve half-metallicity in Heusler alloys, $B2$ -ordering is a sufficient condition; $L2_1$ -ordering is not necessarily required.¹⁴ Possible factors for the increase in TMR ratio are as follows. One is reduction in Mn oxides, which would reduce spin polarization at the interface. The other is intrinsic change in density of states (DOS) in CFMS at E_F , although evident change was not confirmed in differential conductance dependences which will be described later on. Figure 1(c) shows the temperature dependence of the TMR ratio for MTJs with various x . Results show that the temperature dependence of TMR ratio is slightly improved in MTJs with $x=0.4$ and 0.6 compared to other samples with smaller values of x . Considering MTJs with $x=0.8$ and 1.0, the temperature dependence of the TMR ratio is small, although the magnitude of the TMR ratio is also small, as in MTJs with conventional 3d transition metal alloys. To investigate the DOS of ferromagnetic electrode/tunneling barrier interfaces, we measured the differential conductance (dI/dV) of MTJs depending on the applied bias voltage because the tunneling conductance is affected strongly by the DOS at both interfaces especially at parallel magnetic configuration. In Fig. 2, the dI/dV - V spectra of MTJs with parallel magnetic configuration at 2 K are shown. All spectra are normalized at the value of $V=0$ [$(dI/dV)_{V=0}$]. Here, applying positive bias voltage means that the electrons are tunneling from the bottom CFMS electrode to the top Co₇₅Fe₂₅ electrode. For MTJs with $x=0-0.6$, dI/dV is almost constant within a range of $V \sim 0-400$ mV. Such a

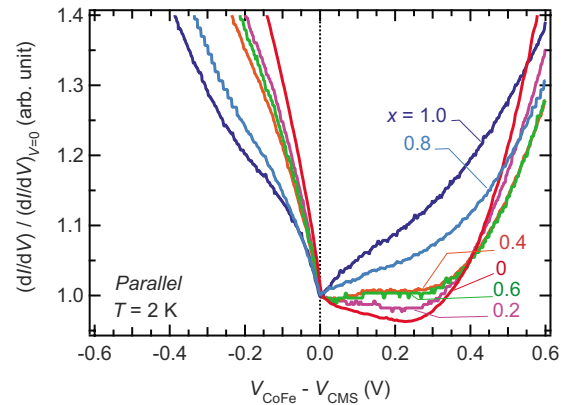


FIG. 2. (Color online) Bias voltage dependence of tunneling conductance (dI/dV) for the MTJs with CFMS/Al–O/Co₇₅Fe₂₅ structures with a parallel magnetic configuration. The measurement temperature was at 2 K; numbers in the figure show the Fe fraction x .

structure is said to originate from the half-metallic energy gap of C(F)MS:¹⁵ the half-metallic energy gap is maintained in Co₂Fe _{x} Mn _{$1-x$} Si films for which the Fe concentration x is 0–0.6. However, for MTJs with $x=0.8$ and 1.0, dI/dV is increased monotonically with increasing bias voltage. Such dependence implies that the half-metallic energy gap disappears in samples with $x \geq 0.8$.

The Gilbert damping constant α was determined at room temperature using FMR measurements with an X-band microwave source ($f=9.4$ GHz) and a TE₀₁₁ cavity. The samples were fixed on a quartz rod. Subsequently, a goniometer was used to measure the out-of-plane angular dependence of the resonance field and linewidth of the FMR spectra. Obtained values of α depending on x are shown on Fig. 3. α has a minimum value of 0.003 at $x=0.4$. Actually, α is inversely proportional to the saturation magnetization (M_s), so to exclude the change of M_s with the variation in film composition, the relaxation frequency $G(=\alpha\gamma M_s)$ of the Heusler alloys (red points) is shown in Fig. 4, which also shows reported values of G for other Co-based Heusler alloys^{16,17} (white circles) as a function of the number of valence electron. Similarly for the dependence of α , G shows the minimum value at $x=0.4$; it increases rapidly for $x > 0.8$. The Gilbert damping constant is considered to be proportional to the square of the spin-orbit coupling parameter ξ and total DOS of d -band at Fermi energy $D(E_F)$.^{17,18} The orbital magnetic moments in Heusler alloys are quite small,¹⁹ which implies that spin-orbit coupling ξ is relatively weak. Additionally, in half-metallic materials, the half-metallic energy gap is around the Fermi level in one spin channel, so that the total DOS might be small. Therefore,

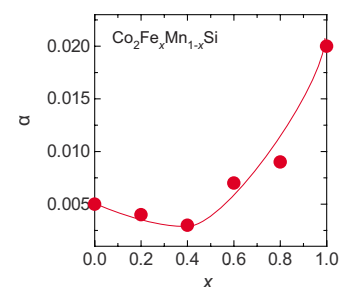


FIG. 3. (Color online) Gilbert damping constants α in Co₂Fe _{x} Mn _{$1-x$} Si Heusler thin films.

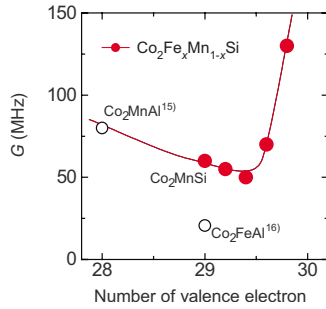


FIG. 4. (Color online) Relaxation frequency $G(=\alpha\gamma M_s)$ for Co-based Heusler alloys with various film compositions. For the number of valence electron=30 (Co_2FeSi), $G=416$ MHz (not plotted in the graph).

Gilbert damping in half-metallic Heusler alloys is expected to be small.

To illustrate the dependence of TMR ratio and G on the CFMS film composition, we propose schematics of DOS in our CFMS samples as presented in Fig. 5. The shape of DOS in Fig. 5 is based on reported calculated results.⁸ Here we are presuming a rigid band model: the energy of the Fermi level is important. Considering the dI/dV spectra in Fig. 2, the CFMS with x of 0–0.6 are apparently half-metallic and the Fermi level is in the gap region. On the other hand, for $x \geq 0.8$, the rapid decrease in the TMR ratio and change in dI/dV spectra imply the rapid increase in minority density of states at the Fermi level. Such descriptions are consistent with the change in Gilbert damping. That is, G is decreased with increasing Fe concentration x in CFMS until x reaches 0.4. Within this region, the DOS in the majority spin channel at Fermi level also decreases concomitantly with increasing E_F (Fig. 5). Then, around $x=0.6$, E_F reaches the edge of the conduction band in the minority spin channel, and G is increased rapidly because of the rapid increase in localized d -states in the minority spin channel.

In our samples, half-metallicity apparently disappears for the sample with $x \geq 0.8$, although some reports show that Co_2FeSi ($x=1.0$) is also a half-metal.^{7,8} The difference between our results and calculations should be discussed with particular care. Possible explanations are the following. First, $L2_1$ -ordering in the current CFMS samples is not perfect. Furthermore, particularly regarding on transport properties, some structural strain might exist especially around the CFMS/Al–O barrier interface. Such factors can narrow the half-metallic energy gap of CFMS and/or shift the Fermi level toward the conduction band. Second, calculations might present some problem. For calculation of DOS in an earlier study,⁸ the LDA+ U method was used. The width of

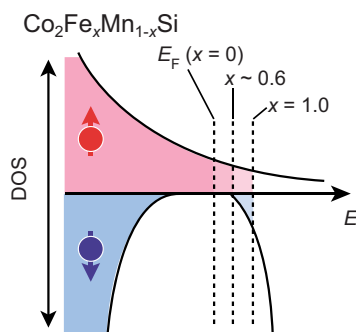


FIG. 5. (Color online) Expected schematic descriptions of density of states for $\text{Co}_2\text{Fe}_x\text{Mn}_{1-x}\text{Si}$. Broken lines respectively denote Fermi levels for $x=0$, about 0.6, and 1.0.

the half-metallic energy gap and the Fermi energy can be changed depending on the effective Coulomb exchange interaction, U . With $U=0$, the conduction band of Co_2FeSi crosses the Fermi level as described in that earlier study. That is, conditions in the theoretical earlier study do not suit the situation in our experimental samples. Such case should also be considered and further investigations are necessary both in theoretical studies and experiments.

In summary, we investigated transport properties of $\text{Co}_2\text{Fe}_x\text{Mn}_{1-x}\text{Si}/\text{Al}-\text{O}/\text{Co}_{75}\text{Fe}_{25}$ MTJs and the Gilbert damping constant in $\text{Co}_2\text{Fe}_x\text{Mn}_{1-x}\text{Si}$ films for x of 0–1.0. The TMR ratio exhibits that a maximum value for x is around 0.4 and 0.6; it reaches 75% at room temperature. The bias voltage dependence of dI/dV spectra imply which half-metallic energy gap exists in samples with x of 0–0.6. The Gilbert damping constant takes a minimum value at x of 0.4. The dependence in the damping constant is consistent with both the expected change in density of states at Fermi level and the transport properties in our MTJs.

Some unknown factors are related to the disappearance of half-metallicity for MTJs with $x=0.8$ and 1.0 remain, although it is interesting that the related behavior of half-metallicity and the Gilbert damping constant depend on film compositions of $\text{Co}_2\text{Fe}_x\text{Mn}_{1-x}\text{Si}$ Heusler epitaxial thin films.

This work was partly supported by a research fellowship for young scientists from the Japan Society for the Promotion of Science (JSPS) and the New Energy and Industrial Technology Development Organization (NEDO).

- ¹S. Ishida, S. Fujii, S. Kashiwagi, and S. Asanok, *J. Phys. Soc. Jpn.* **64**, 2152 (1995).
- ²I. Galanakis, P. H. Dederichs, and N. Papanikolaou, *Phys. Rev. B* **66**, 174429 (2002).
- ³Y. Sakuraba, T. Miyakoshi, M. Oogane, Y. Ando, A. Sakuma, T. Miyazaki, and H. Kubota, *Appl. Phys. Lett.* **88**, 192508 (2006).
- ⁴T. Ishikawa, T. Marukame, H. Kijima, K.-I. Matsuda, T. Umemura, M. Arita, and M. Yamamoto, *Appl. Phys. Lett.* **89**, 192505 (2006).
- ⁵S. Tsunegi, Y. Sakuraba, M. Oogane, K. Takanashi, and Y. Ando, *Appl. Phys. Lett.* **93**, 112506 (2008).
- ⁶P. J. Webster, *J. Phys. Chem. Solids* **32**, 1221 (1971).
- ⁷S. Wurmehl, G. H. Fecher, H. C. Kandpal, V. Ksenofontov, C. Felser, H.-J. Lin, and J. Morais, *Phys. Rev. B* **72**, 184434 (2005).
- ⁸H. C. Kandpal, G. H. Fecher, C. Felser, and G. Schonhense, *Phys. Rev. B* **73**, 094422 (2006).
- ⁹M. Oogane, M. Shinano, Y. Sakuraba, and Y. Ando, *J. Appl. Phys.* **105**, 07C903 (2009).
- ¹⁰G. M. Müller, J. Walowski, M. Djordjevic, G.-X. Miao, A. Gupta, A. V. Ramos, K. Gehrke, V. Moshnyaga, K. Samwer, J. Schmalhorst, A. Thomas, A. Hütten, G. Reiss, J. S. Moodera, and M. Münzenberg, *Nature Mater.* **8**, 56 (2009).
- ¹¹R. Yilgin, Y. Sakuraba, M. Oogane, S. Mizukami, Y. Ando, and T. Miyazaki, *Jpn. J. Appl. Phys., Part 2* **46**, L205 (2007).
- ¹²J. C. Slonczewski, *J. Magn. Magn. Mater.* **159**, L1 (1996).
- ¹³M. Oogane, T. Kubota, N. Hirose, and Y. Ando, "Magnetic damping constant of Co_2FeMnSi Heusler alloy thin films," *J. Magn. Soc. Jpn.* (in press).
- ¹⁴Y. Sakuraba, M. Hattori, M. Oogane, H. Kubota, Y. Ando, A. Sakuma, N. D. Telling, P. Keatley, G. van der Laan, E. Arenholz, R. J. Hicken, and T. Miyazaki, *J. Magn. Soc. Jpn.* **31**, 338 (2007).
- ¹⁵Y. Sakuraba, T. Miyakoshi, M. Oogane, Y. Ando, A. Sakuma, T. Miyazaki, and H. Kubota, *Appl. Phys. Lett.* **89**, 052508 (2006).
- ¹⁶R. Yilgin, M. Oogane, S. Yakata, Y. Ando, and T. Miyazaki, *IEEE Trans. Magn.* **41**, 2799 (2005).
- ¹⁷S. Mizukami, D. Watanabe, M. Oogane, Y. Ando, Y. Miura, M. Shirai, and T. Miyazaki, *J. Appl. Phys.* **105**, 07D306 (2009).
- ¹⁸V. Kambersky, *Can. J. Phys.* **48**, 2906 (1970); B. Heinrich, in *Ultrathin Magnetic Structures*, edited by J. A. C. Bland and B. Heinrich (Springer, New York, 2005), Vol. 3.
- ¹⁹I. Galanakis, *Phys. Rev. B* **71**, 012413 (2005).